Check for updates

RESEARCH ARTICLE

ADVANCED ELECTRONIC MATERIALS
Open Access
www.advelectronicmat.de

Analysis of the Electrical ReRAM Device Degradation Induced by Thermal Cross-Talk

*Mohammad Al-Mamun, Amrita Chakraborty, and Marius Orlowski**

A switching of resistive memory cells leads to a local accumulation of Joules heat in the device. In resistive RAM (ReRAM) arrays, the heat generated in one cell spreads via common electrode metal lines to the neighboring cells and may cause their performance degradation. The performance degradation results in reduced number of switching cycles and, in extreme cases, even in a loss of a bit, caused by the rupture of the nanofilament. The authors propose a thermal analysis of the thermal cross-talk, describe its impact on cells' electric performance, and identify three major mechanisms for the ReRAM reliability: (i) thermal conductivity, (ii) the specific heat capacity, and (iii) geometry of the electrodes. Several ReRAM arrays are manufactured to vary thermal conductivity, specific heat and geometry of the electrodes by depositing eight different inert electrodes: Pt(50 nm)/Ti(30 nm), Ru(50 nm)/Ti(30 nm), Co(50 nm)/Ti(30 nm), Pt(50 nm/Cu(100 nm)/Ti(30 nm), Pt(50 nm)/ Cu(200 nm)/Ti(30 nm), Ru(50 nm/Cr(30 nm), Ru(50 nm)/Ti(50 nm), and Rh(50 nm)/Cr(30 nm). The experimentally found differences of the degradation of electric performance of the array cells performed under identical circumstances can be correctly predicted by the proposed thermal analysis using the material properties and geometry parameters of the electrodes.

1. Introduction

Traditional non-volatile memory based on floating gate MOSFET transistor has reached its scaling limits, and, hence, the development of alternative memory cells has become imperative. Resistive Random Access Memory (ReRAM) is one of the prime candidates to replace the current non-volatile technology due to its simple architecture, excellent scaling potential, low power consumption, high switching speed, large on/off ratio and good retention, and endurance properties.[1–3] Resistive memory cells hold also promise for neuromorphic applications.[4,5] A comprehensive recent review of different types of volatile and nonvolatile memristive devices and of their suitability for neuromorphic computing has been given by G. Zhou et al.[6] Memristive devices enable also second-order associative memory circuits holding promise to mimick the function of the human brain including functions of forgetting and learning.[7] The resistive switching device is a two-terminal device, such as Cu/TaO_x/Pt, composed of a solid electrolyte insulating layer (here TaO_x) sandwiched between two metal electrodes. The solid electrolyte layer displays a change between high and low resistance states in response to a suitably applied electric field. In so called bipolar resistive devices, the transition from a low resistance state (LRS), characterized by the resistance R_{on} to a high resistance state (HRS), characterized by the resistance R_{off}, occurs at an opposite polarity than the switching from HRS and LRS. The resistance switching effect is ascribed to the formation and rupture of conductive nano-filaments (CF) in the insulating material matrix due to ionic and charged defect electromigration and to the thermal effects.[8] In the case of so called electrochemical metallization[9] responsible for the formation of a metal atom CF, metal cations of the active electrode (here Cu) drift in the electric field toward the also called inert electrode (here Pt, Ru, Co, Rh), where they are stopped and neutralized. Over time, the Cu metal atoms pile up on the Pt interface and form a metal nanofilament between the two electrodes. This process constitutes the so-called SET operation. In contrast, when a negative voltage is applied to the active electrode, a large current is flowing through the filament depositing Joule heat and causing the Cu atoms to diffuse out leading to the rupturing of the filament at a critical current I_{reset}. The rupturing of the filament is called the RESET operation. Especially, during the RESET operations, Joule heating is of crucial importance. It has been amply demonstrated[10–14] that the RESET process is dominated by Joule heating. The self-heating effects associated with the switching of the cell lead to the deterioration of the R_{off}/R_{on} ratio[15] since for the off-state associated with a semiconductor behavior, i.e., resistance R_{off} decreases as the temperature increases, while the on-state exhibits metallic behavior with the resistance R_{on} increasing with increasing

M. Al-Mamun, A. Chakraborty, M. Orlowski
Bradley Department of Electrical and Computer Engineering
Virginia Tech
Blacksburg, Virginia 24061, USA
E-mail: m.orlowski@vt.edu

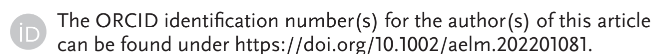
The ORCID identification number(s) for the author(s) of this article can be found under https://doi.org/10.1002/aelm.202201081.

© 2023 The Authors. Advanced Electronic Materials published by Wiley-VCH GmbH. This is an open access article under the terms of the Creative Commons Attribution License, which permits use, distribution and reproduction in any medium, provided the original work is properly cited.

DOI: 10.1002/aelm.202201081

2199160x, 0, Downloaded from https://onlinelibrary.wiley.com/doi/10.1002/aelm.202201081 by Virginia Tech, Wiley Online Library on [23/03/2023]. See the Terms and Conditions (https://onlinelibrary.wiley.com/terms-and-conditions) on Wiley Online Library for rules of use; OA articles are governed by the applicable Creative Commons License

ADVANCED
ELECTRONIC
MATERIALS
Open Access
www.advelectronicmat.de

temperature. Walczyk et al[15] found that the R_{off}/R_{on} ratio decreased from a value of 20 to ≈5 over the temperature interval of 213K-413 K. Such changes in R_{on} and R_{off} of ReRAM cells also cause significant degradation in the computational accuracy of ReRAM based neuromorphic computing systems.[5,6] Specifically, a hotter cell is more susceptible to generate an incorrect output. The thermal reliability of ReRAM is also a concern for embedded memories for automotive applications.[16] Chang et al[14] found two different modes of resistive switching for identical devices with the exception of a different thickness of the bottom Pt electrode. The difference in switching behavior has been explained in terms of the temperature-dependent stability of the CF. Thinner thickness of the bottom electrode makes the dissipation of Joule heat less efficient and hence the filament will be heated to a higher temperature and become more unstable at the same switching conditions. A comprehensive review of resistive switching phenomena has been given.[17]

Switching of a cell repeatedly leads to an increasing deposition of Joule heat in the device. It has been shown[18,19] that the Joules heat is transported preferentially along the electrode metal lines affecting the neighboring cells disposed along the same electrode lines and causing the deterioration of their electrical properties. Moreover, it has been shown[19,20] that the thermal cross-talk can erase a programmed neighboring cell, if the nanofilament in the cell is fragile enough and sufficient amount of heat has been transferred to it from the heated cell. For some combinations of specific amount of heat transfer and the strength of the Cu filament, the bit of the cell may be erased temporarily by remote heating. The filament recovers spontaneously after a couple of tens of seconds.[19,20]

The goal of this work is to provide a thermal analysis explaining the various electric degradation phenomena in terms of material properties and geometries of the electrodes of the memory cells.

2. Experimental Section

In the most common architecture, ReRAM cells lie at the intersection of perpendicular metal electrode lines in a crossbar array as shown in **Figure 1**a. The cross-section of the baseline $Cu/TaO_x/Pt/Ti$ and of the derivative ReRAM devices shown in **Figure 2** was fabricated in a crossbar array on a thermally oxidized Si wafer[3] with a SiO_2 layer with 730 nm thickness. Notably, the seven different devices differed only in the construction of the inert electrode. Cu (150, 100, and 200 nm), Pt (50 nm), Rh(50 nm), Co(50 nm), Ru(50 nm), Cr(30 nm), and Ti (30 nm) layers were deposited in a Kurt Lesker e-beam PVD-250 chamber and patterned by lift-off technology with a photoresist thickness of 2 µm to make sure that the sidewalls are sloped gently. A thin Ti or Cr layer of 30 nm was used between Pt, Ru, Rh, Co, and SiO_2 to improve the adhesion of the inert electrode proper layer and also to modulate the thermal properties of the composite electrode. The thickness of TaO_x was 25 nm. The thickness of the TaO_x on the sloped sidewalls of Pt line was 98% of the planar thickness as confirmed by Ta_2O_5 atomic layer cells manufactured with Ta_2O_5 deposition by atomic layer deposition (ALD).[21] The oxygen-deficient TaO_x ($x \approx 1.9$) was deposited also in the PVD-250 chamber by evaporating Ta_2O_5 pellets without O_2 injection into the evaporation chamber. The details of the sample manufacturing process were given,[21] where the role of the parameter x in TaO_x (as opposed to the stoichiometric Ta_2O_5) on resistive switching properties has been discussed in detail. The width of metal lines varied between 5 and 35 µm resulting in rectangular device areas of the device in the range of (5 to 35) x (5 to 35) μm^2. The neighboring line pitch was 150 µm and the lateral dimensions of the contact pads were 100 µm × 100 µm.

To protect the manufactured memory arrays from damages by moist environment,[22] the manufactured devices were kept in a desiccator in a clean room. The memory cells used in this investigation are described in much detail.[23,24]

The electrical characterization was performed at room temperature on a probe station equipped with Keithley 4200-SCS analyzer. To set the ramp rate, Keithley equipment allows one to choose the voltage step height and it automatically determines the pertinent time step. As an example, if a step height of 0.025 V is selected, the Keithley analyzer returns a time step of 80 mV, resulting in a ramp rate of 0.313 V s^{-1}.

When a positive voltage is applied to the Cu electrode, Cu cations are generated according to the redox reaction:

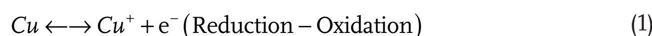

$$Cu \longleftrightarrow Cu^{+} + e^{-} \, (\text{Reduction} - \text{Oxidation}) \quad (1)$$

and migrate under the influence of the electric field in the solid electrolyte to be electrochemically reduced on the surface of the Pt, Ru, Rh, Co cathode which acts as an effective

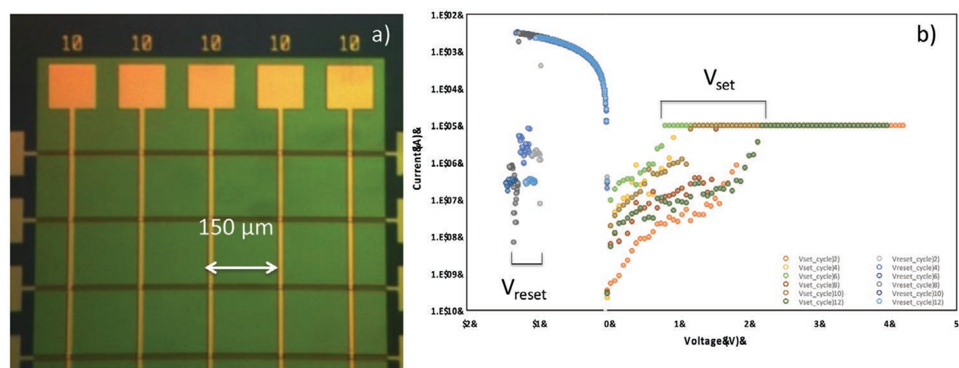

Figure 1. a) Optical micrograph of the crossbar architecture of $Cu/TaO_x/(Pt,Rh,Ru)$ devices. b) Even cycles of a typical first 12 switching set and reset cycles of a $Cu/TaO_x/Pt$ device.

© 2023 The Authors. Advanced Electronic Materials published by Wiley-VCH GmbH

2199160x, 0, Downloaded from https://onlinelibrary.wiley.com/doi/10.1002/aelm.202201081 by Virginia Tech, Wiley Online Library on [23/03/2023]. See the Terms and Conditions (https://onlinelibrary.wiley.com/terms-and-conditions) on Wiley Online Library for rules of use; OA articles are governed by the applicable Creative Commons License

2199160x, 0, Downloaded from https://onlinelibrary.wiley.com/doi/10.1002/aelm.202201081 by Virginia Tech, Wiley Online Library on [23/03/2023]. See the Terms and Conditions (https://onlinelibrary.wiley.com/terms-and-conditions) on Wiley Online Library for rules of use; OA articles are governed by the applicable Creative Commons License

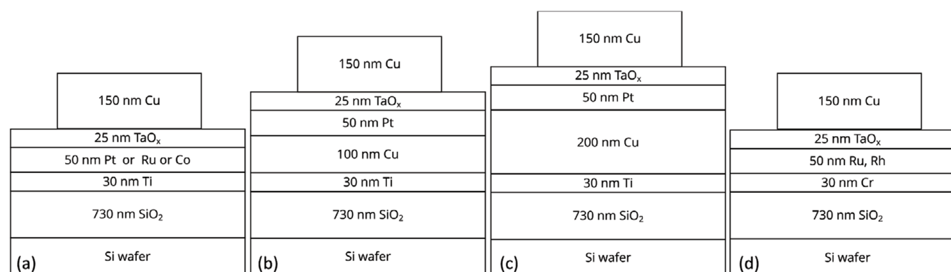

Figure 2. Four different types of ReRAM arrays considered in this work, which are manufactured, characterized, and analyzed in this work. All devices have the same TaOx switching layer and the same active Cu electrode with 150 nm thickness. They differ only in the inert electrode (IE). Type (a) encompasses four devices Cu/TaO_x/Pt/Ti, Cu/TaO_x/Ru/Ti, and Cu/TaO_x/Co(50 nm)/Ti(30 nm). Type (b) shows a device with Pt(50 nm)/Cu(100 nm)/Ti(30 nm), i.e., Type (c) shows a device with Pt(50 nm)/Cu(200 nm)/Ti(30 nm), i.e., Type (d) encompasses two devices with Cr as a glue layer instead of Ti with IE: Ru(50 nm)/Cr(30 nm) and Rh(50 nm)/Cr(30 nm). In total, eight different CuTaO_x/IE with seven different inert electrodes have been manufactured, characterized and analyzed in this work. The inert electrodes display different thermal properties, summarized in Table 2.

diffusion barrier for Cu atoms. As more and more Cu atoms accumulate, the copper atom protrusion grows and a metallic filament (CF) of Cu atoms as building blocks forms a conductive path between two electrodes. An abrupt onset of conductance occurs at a threshold voltage V_{set}. The filament can be partially undone by applying a negative voltage to the Cu electrode and grounding the inert electrode. The abrupt rupturing of the filament occurs in the I-V characteristics at a threshold voltage, V_{reset}. Several typical I-V characteristics for set and reset operations are shown in Figure 1b. Before a measurement is taken, the two grounded needles were placed on the cell contacts for at least 20 s to make sure that the cell capacitor is fully discharged. Then, for the SET operation, the voltage of the Cu electrode starting at 0 V was ramped at a ramp rate (rr) ranging from 0.01 V s^{-1} to 2.50 V s^{-1}. During the SET operation, a compliance current (I_{cc}) of 5 µA to 1 mA were imposed without an off-chip resistance lest the device be damaged. This work is interested in cells that have been set prior to the heating of a neighboring (heated) cell into a LRS state under various levels of compliance current, I_{cc} and that are connected by a thermal path to the heated device as shown in **Figure 3**.

Since this paper is concerned with thermal properties of the electrodes, and particularly of the inert electrode, **Table 1** summarizes the important material properties of the materials involved in manufacturing of the devices shown in Figure 2. Since several inert electrodes are composite electrodes and in order to expedite the thermal analysis given below, the effective thermal conductivity for the composite inter electrodes was calculated. The effective thermal conductivity was calculated as a weighted average of the respective layer thicknesses and is shown in **Table 2**.

It is known that the imposition of I_{cc} during the set operation controls the resistance of the LRS state, R_{on}, via the relation:[2]

$$R_{on} = K/I_{cc}^{n} \tag{2}$$

where K extracted from experimental data for the Cu/TaO_x/Pt devices yields K ≈ 0.29 V and n ≈ 1. It has been shown[2] that the constant K for n = 1 represents the minimal voltage under which the device can be set. A typical R_{on} on I_{cc} dependence is shown for Cu/TaO_x/Pt/Ti devices in **Figure 4**.

This was confirmed following the procedure outlined[2] by applying a constant voltage to a reset cell and measuring the current as a function of time. For all voltages in excess of 0.287 V, the cell can be set to an ON-state, whereas for voltages smaller than 0.287 V, the cell remains in the OFF-state, even when the voltage is applied for a long period of time. The dependence of R_{on} on I_{cc} allows one to form stable but weak, i.e., highly resistive (R_{on} = 50 kΩ) Cu filaments at I_{cc} = 5 µA, and strong, low resistive (R_{on} = 500 Ω) Cu The filaments at I_{cc} = 0.2 mA. For compliance current values below 5 µA, the filament did not form at all or became volatile and ruptures unaided and spontaneously. On the other hand, robust low-resistance Cu filaments formed at I_{cc} > 0.25 mA were prone to become inoperable, i.e., meaning that the cell has been permanently damaged (shorted).

The retention properties of all devices has been found to be satisfactory. **Figure 5** shows the retention of Ru and Pt devices

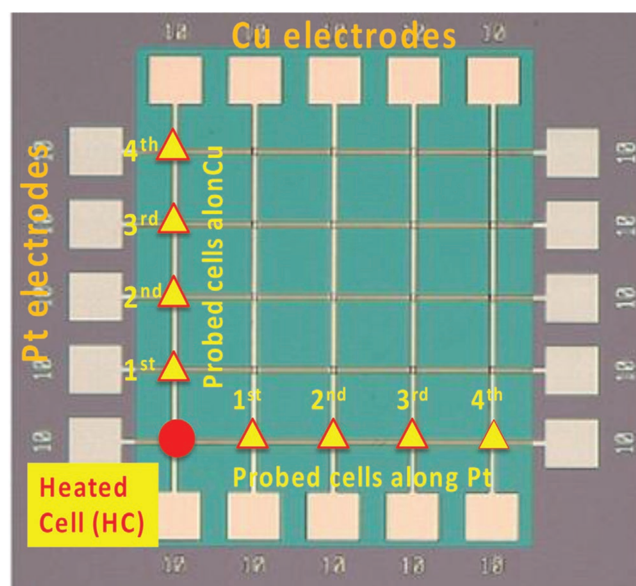

Figure 3. A Cu/TaO_x/Pt crossbar array shown in the optical micrograph with heat source cell and neighboring cells indicated. The cell marked by the red dot represents the heat source cell. The neighboring cells affected by the heat source are disposed along the Cu and Pt line and marked by black crosses. The neighboring probed cells are set prior to heating by cell A to an OFF-state. Immediately after the heating by the heated cell has ended, the neighboring cells are tested to find their maximum switching cycles.

 © 2023 The Authors. Advanced Electronic Materials published by Wiley-VCH GmbH

ADVANCED ELECTRONIC MATERIALS Open Access
www.advelectronicmat.de

Table 1. Relevant properties (mass density, resistivity, thermal conductivity, specific heat capacity, and thermal diffusivity of materials of ReRAM arrays manufactured and analyzed in this work.

Material	Mass density [g/cm^3]	Resistivity [Wcm]	Thermal conductivity [W/(m °K]	Specific heat capacity [J/(g °K]	Thermal diffusivity [cm^2/s]
Cu	9.0	1.7×10^{-6}	396	0.395	1.11
Pt	21.7	10.6×10^{-6}	69	0.134	0.24
Rh	12.4	4.3×10^{-6}	150	0.242	0.5
Co	8.9	6.2×10^{-6}	69	0.419	0.19
Ru	12.4	7.1×10^{-6}	116	0.239	0.39
Ti	4.5	42.0	18	0.544	0.07
Cr	7.2	12.5	94	0.460	0.28

(a) for the on-state characterized by R_{on}, and (b) for the off-state characterized by R_{off}. It can be seen from Figure 5 that the level of noise for Ru devices is higher than for Pt devices for both bit states, characterized by R_{on} and R_{off}. While R_{off} fluctuations of Ru devices are irrelevant as the outlier lie in the tens of GΩ range, the outliers for R_{on} are more of a concern, as its variation can be as high as 75%. Such large fluctuations could pose, inter alia, a problem for the multibit storage applications and for the stability of the sense amplifiers when reading the cell. For comparison the variations of R_{on} and R_{off} in Pt devices are less than 10% as discussed in more detail.[26]

As described in more detail,[8,19] a frequent switching of a cell led to a deposition of Joules heat in that cell that can spread to neighboring cells disposed along one of the electrodes shared with the heated cell. Even those cells that do not share any of the two electrodes with the heated cell can be affected by the thermal cross-talk provided the intermediate cells are set in the ON-state whereby the Cu filament provides a thermal conduit for the heat transport. This phenomenon allowed remote heating of neighboring cells to a various degree dependent on the amount of heat dissipated in the heated cell, on the selected shared electrode and the distance of the cell from the heated cell, see Figure 3.

Several thermal models have been put forward in the literature to estimate the temperature distribution in ReRAM cells. G. Zhou et al[6] discussed how localized Joule heat affect the strength of the CF. Mickel et al[26] proposed a geometrically equivalent circuit to calculate the heat transport through the conductive filament, yielding temperature distribution of the memory cell as a function of the spatial dimensions. The critical temperature responsible for the rupturing of a filament was calculated to be ≈1225 °K. In another work, Mickel et al[27] proposed a set of constitutive equations describing the evolution of the heat transport. Based on this approach, the temperature responsible for the rupturing of the filament may be even as high as ≈1500 °K. Sun et al[28] also found that the peak temperature of the filament is somewhere between 600 °C and 900 °C. Most of the models assumed a thermal boundary condition at the mesoscopic electrodes to be the room temperature. These results clearly refuted this assumption. The electrode lines were heating up considerably and enabled the thermal cross-talk between the cells of the array. Karpov et al[29] discussed a thermal model for a metallic filament with the temperature boundary condition other than room temperature that is adequate to the thermal crosstalk situation. Fangohr et al[30] investigated Joule heat in nanowires with various constriction geometries and found that the temperature at the constriction is as high as 1336 °K. Uenuma et al.[31] observed by infrared detection the position of the CF from Joule heating at the surface of the electrode on the CF and estimated the temperature to be larger than 900 °C. Sato et al.[32] found that the temperature in the reset process reaches the same temperature level in each reset and estimated the temperature of filaments with radii 10 nm – 40 nm to be between 1000 °C and 1200 °C, depending on the resistivity of the filament. Thus, there is a wide consensus that the local peak temperature of the filament can be very high and this temperature is bound to increase further when the cell is switched on and off sequentially with high switching frequency. This work presents an experimental evidence that a strongly heated cells may lead to local melting of the Cu electrode at 1085 °C.

3. Thermal Cell-to-Cell Cross Talk Effects in ReRAM Arrays

Switching of a cell repeatedly leads to an accumulation of depositions of Joules heat in the device. The heating of the cell was accomplished by applying N set-reset cycles. It is noted that during a set cycle, the heat dissipation is very small and negligible compared with the reset cycle. During the set operation before V_{set} is reached the current is below 1 nA, and when threshold voltage is reached the current is limited in our experiments by I_{cc} to less than 100 µA, whereas the current during the reset operation is in the mA range. Therefore, the heating occurs predominantly during the reset operation and can be represented by heat pulses of a pulse duration of several seconds (t_{res}) with a pulse period of 40–60 s, the time needed to operate the probe station in different bias conditions. This means that during the reset operations when the cell is heated

Table 2. Effective thermal conductivity of composite electrodes and Cu electrode. The thickness of a specific metal layer is indicated in units of nm. The effective thermal conductivity has been calculated as a weighted average of the layer thickness.

Electrode [nm]	Cu150	Pt50Ti30	Pt50Cu100	Pt50Cu200	Ru50Ti30	Ru50Cr30	Rh50Cr30	Co50Ti30
eff. m_{th} [W/mK]	389	50	282	325	81	110	79	50

© 2023 The Authors. Advanced Electronic Materials published by Wiley-VCH GmbH

2199160x, 0, Downloaded from https://onlinelibrary.wiley.com/doi/10.1002/aelm.202201081 by Virginia Tech, Wiley Online Library on [23/03/2023]. See the Terms and Conditions (https://onlinelibrary.wiley.com/terms-and-conditions) on Wiley Online Library for rules of use; OA articles are governed by the applicable Creative Commons License

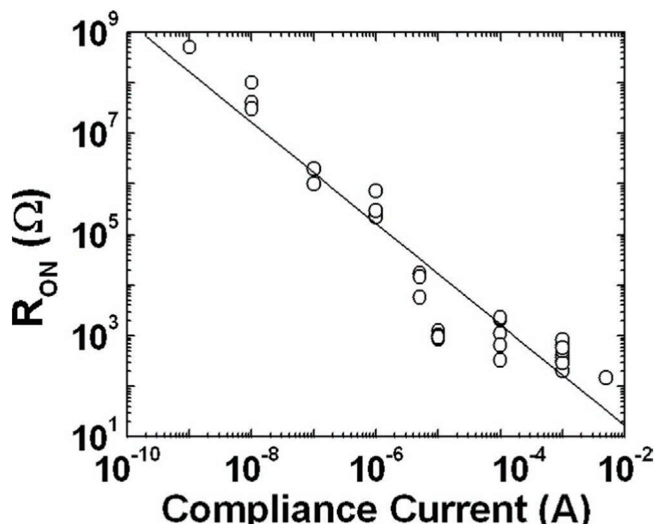

Figure 4. Dependence of on-resistance R_{on} on compliance current I_{cc} for Cu/TaO_x/Pt device.

up, there follows a prolonged cool-off period of ≈40 s. Thus, the duty cycle of the heating is smaller than ≈0.05. During the off pulse time, the cell and the system will cool off due to Newtonian losses, but not completely. The fraction of the heat retained in the cell is only a fraction of the heat deposited; this fraction is described by the factor f_{loss}. Therefore, several cycles are needed to accumulate enough heat in the device to reach a certain temperature. It has been recently shown[18,19] that the Joules heat is transported along the shared electrode metal lines, which affects the neighboring cells and causes the deterioration of their electrical properties.[19] The heat generated in the heated memory cell can be controlled by the voltage ramp rate, rr, applied during the reset operation and by the number, N, of consecutive set-reset cycles, and by the R_{on} resistance of the Cu CF.

During the electrical characterization of the memory cells, it has been noticed that the electrical switching of a fresh cell has been degraded when a direct neighbor of this cell, has been heated by repeated SET-RESET cycles. The degradation manifests itself by the onset of volatility after the device has been cycled only a few times. This degradation of electrical properties disappeared when the cell was tested again after 5 min or a longer cool-off time period. We assume that the thermally induced degradation subsides after times of the order of 2–5 min. Tests between various Pt and Cu line proved that no sneak paths[33] are present.

In order to quantify the thermal cross talk, a metric of so called "marginal" memory cell has been introduced.[18,19] By a cell being "marginal" we mean following cell's behavior after being subject to a specific SET condition: We set a device at an I_{cc} of only 10 µA and a voltage ramp rate rr = 1.1 V s^{-1}. When the cell is set at such conditions, the cell becomes volatile after a limited number of sequential SET-RESET switching cycles. One manifestation of volatility are spontaneous RESET events. The marginality of the device is demonstrated further when the device is set at slightly lower and slightly higher I_{cc}. When applying I_{cc} < 7 µA, the device cannot be set permanently in a LRS state. When the same device is set at higher compliance currents of 8–10 µA, the LRS state is stable although only for a very small number of sequential switching cycles, typically 11–14, after which the cell becomes volatile, eventually. A test has been applied to ≈100 cells set at I_{cc} = 10 µA and a maximum of consecutive switching cycles has been determined. We obtain a mean of M_x = 12.7 cycles and standard deviation σ = 1.3. The cells set at I_{cc} = 10 µA display a rather tight distribution of R_{on} values with the mean value of 27.7 kΩ with a standard deviation, σ = 13.2 kΩ.

A low rr = 0.1 V s^{-1} has been applied during the RESET operation to allow for a long heating time. For a low rr, the current lingers for a long time and hence low rr maximizes heat dissipation. In[34] it has been shown that V_{reset} decreases with decreasing ramp rate, rr, as $V_{reset} \sim \sqrt[3]{rr}$ When the maximum number of switching cycles (M_x) is reached, the device is driven to a highly unstable performance. On the other hand, a device set at I_{cc} = 40-100 µA can be switched repeatedly more than hundreds of times. Thus, a "marginal" device demarcates the boundary between stable and unstable (volatile) behavior of the cell. Hence, a "marginal" device set at I_{cc} = 10 µA is our "canary in the coal mine" and the maximum number of switching cycles, M_x, is our metric to quantify the degree of the thermal cross talk. We find that such a marginal device when heated remotely by another cell will have a maximum number of switching cycles smaller than M_x = 13, depending on the amount of heating experienced from the heated cell. Thus, the measure M_x defines the onset of the cell's volatility in response to the local temperature of the cell. Thus, the remote heat superposes on the heat generated locally by the switching of the cell itself. In our experimental setup, the time between stop of the heating of the heated cell and characterization of the

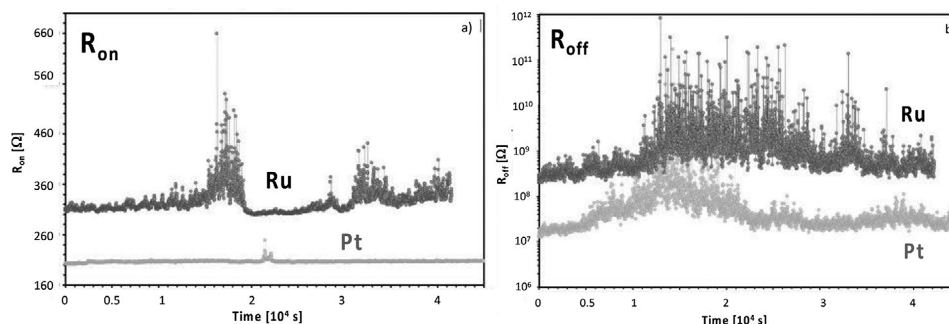

Figure 5. Retention of Ru and Pt devices a) for the on-state characterized by R_{on}, and b) for the off-state characterized by R_{off}.

© 2023 The Authors. Advanced Electronic Materials published by Wiley-VCH GmbH

2199160x, 0, Downloaded from https://onlinelibrary.wiley.com/doi/10.1002/aelm.202201081 by Virginia Tech, Wiley Online Library on [23/03/2023]. See the Terms and Conditions (https://onlinelibrary.wiley.com/terms-and-conditions) on Wiley Online Library for rules of use; OA articles are governed by the applicable Creative Commons License

2199160x, 0, Downloaded from https://onlinelibrary.wiley.com/doi/10.1002/aelm.202201081 by Virginia Tech, Wiley Online Library on [23/03/2023]. See the Terms and Conditions (https://onlinelibrary.wiley.com/terms-and-conditions) on Wiley Online Library for rules of use; OA articles are governed by the applicable Creative Commons License

probed cell is ≈50s – the time required to replace the needles on the probe station.

The metric for degradation is established customarily by relating the M_x for the remotely heated cell to M_x of an unheated cell as:

$$D = \frac{M_x(\text{unheated cell}) - M_x(\text{heated cell})}{M_x(\text{unheated cell})} \quad (3)$$

The mean of M_x for an unheated cell has been found to be 13 SET-RESET cycles, as mentioned before. The cell degradation results for cells disposed along the Pt and Cu electrodes are shown in **Table 3** based on 125 devices measured. It can be seen that for the nearest neighbors the degradation is about D = 67%. In contrast, the degradation of the 4th device located on the Pt electrode is much smaller, D = 13%. The results will be explained below by the heat transfer over a distance of n × 150 µm where n = 1,2,3,4, corresponding to the 1st, 2nd, 3rd, 4th neighboring cell as shown in Figure 3. The degradation of electrical performance of the neighboring cells due to thermal cross-talk is shown in Table 3.

As discussed extensively in[19] Table 3, it is seen that the degradation of the neighboring cells along the Cu electrode is much more pronounced than of the neighboring cells along the Pt electrode. The finding that the degradation along the Pt electrode is smaller than along the Cu electrode was, at first, surprising[19] as one would assume that the Cu filament has a broad base with the Pt electrode while a small contact area at the tip of a truncated cone with the Cu electrode. The increased degradation along the Cu line led to the revision of the shape of the filament from a come to more an hourglass shape[19] which has large contact area with both electrodes. The reason for the larger degradation of the devices along the Cu electrode is the much higher rate of heat transfer along the Cu electrode than along the Pt electrode. The rate of heat transfer is proportional to the product of thermal conductivity and the cross-section area of the electrode. The thermal conductivity of Cu is almost 8 times larger than of Pt/Ti see Table 2 and the cross-section of the Cu electrode is 2.5 times larger than that of the Pt/Ti electrode. Therefore the rate of heat transfer along the Cu electrode is more than 20 times larger than along the Pt electrode. Consequently, the neighboring cells along the Cu electrode are heated up to higher temperatures than along the Pt electrode.

4. Thermal Analysis, Predictions of ReRAM cells' Degradation and Verification

The heating of the cell A can be controlled by a number of sequential switching (set-reset) cycles, N, the level of I_{cc}, and by the voltage ramp rate, rr, during the reset cycles. To maximize the heating, a high I_{cc} leading to a robust low resistance Cu CF, and/or by a low rr = 0.1 V s^{-1} may be chosen for the reset operation providing a long heating time prior to reaching the threshold voltage V_{reset}. For a low rr, the current lingers for a long time and hence low rr maximizes heating of the cell. For a cell to which a constant voltage ramp rate is applied, the Joules heat Q_{JH} can be calculated by Equation (4)[34,35] where relation between R_{on} and I_{cc} (see Equation (2)) has been used to obtain the final expression.

$$Q_{JH} = \int_0^{t_{res}} \frac{V^2(t)}{R_{on}} dt = \int_0^{V_{res}/rr} \frac{rr^2 \times t^2}{R_{on}} dt = \frac{V_{res}^3 \times I_{cc}}{3 \times rr \times K} \quad (4)$$

Here the reset time, t_{res}, at an applied voltage ramp rate rr is given by $t_{res} = V_{res}/rr$.[34,35] Depending on the chosen values for I_{cc} and rr, Q_{JH} can vary from 3 to 60 µJ.

Q_{JH} is the energy that went into the memory array and is solely determined by external parameters, the applied voltage ramp rate rr, and the experimental values for R_{on} and V_{reset}. The primary locus of the heat generation is the nanofilament characterized by the on-resistance R_{on}. Since the nanofilament is totally encapsulated in the memory cell, the question arises where the generated heat is being stored. The heat transferred to a material increases the material's temperature according to Equation (5)

$$Q = c_s \times m \times \Delta T \quad (5)$$

where c_s is specific heat of the material, m is the mass of the material, and ΔT is the temperature difference, with a reference temperature of the room temperature of the device.

In evaluating Equation (5), one has to take into account the temperature dependence of the specific heat capacity which – for an exact solution – would require numerical solution.[37] The heat capacity of metals varies with temperature according to the Debye theory and displays strong dependence with up to slightly below the Debye temperature, T_D, of the material.[36] Around and above T_D, the specific heat capacity of metals increase only modestly with increasing temperature. For example, the specific heat capacity for Cu and Pt increases from T = 300 °K T = 1350 °K by 16%. Since T_D(Pt) = 240 °K and T_D(Cu) = 340 °K, and the temperature interval of operation of our ReRAM devices is 300 °K–1350 °K, a constant specific heat capacity appears to be an acceptable 1st order approximation. Because the heat capacity is slightly underestimated in our estimates at high temperatures, our ΔT values at high temperatures are slightly overestimated by the same percentage.

Among other things, Equation (5) indicates that the increase of the temperature difference ΔT depends on the shape of the electrode. In order to evaluate Equation (5) for a given heat generated, one needs to calculate the total mass of the electrode

Table 3. The average maximum number of switching cycles, M_x(ave) and degradation, D, of the neighbor cells of the heated device for the array with inert electrode of Pt(50 nm) array for a 10 mm wide line.[19]

#neighbor	Neighbor cell to the heated cell along Pt(50 nm)/Cu(0 nm) metal line				Neighbor cell to the heated cell along Cu metal line			
	1st	2nd	3rd	4th	1st	2nd	3rd	4th
M_x (ave)	4.8	6.1	7.8	11.3	2.6	3.3	3.9	4.3
D [%]	67	53	40	13	80	75	70	67

© 2023 The Authors. Advanced Electronic Materials published by Wiley-VCH GmbH

which is given by the product of mass density times the total volume of the electrode (width × length × thickness) including the volume of the connected contact pads. Clearly, the thicker or wider the electrode is, the larger its mass, and the smaller the temperature increase, ΔT. Hence the geometry, i.e., the volume of the electrode, determine the amount of the temperature increase ΔT.

Let us assume for a moment that the heat Q_{JH} generated in the filament is stored entirely in the Cu nanofilament. One may ask then, what the temperature difference would be in order to accommodate a heat of 10 µJ in a Cu NF. In order to answer it, one has to calculate the volume of the Cu NF, estimate its mass density, and its specific heat. Assuming a truncated cone shape of nanofilament with a radius of 8 nm at the bottom, and 5 nm top radius, and 25 nm height, given by the thickness of the TaO_x, the volume comes to 4.6×10^{-18} cm^3.[37] This volume and geometry lead to a R_{on} resistance of ≈1000 Ω, if one assumes the resistivity of the Cu NF of 5×10^{-4} Ωcm, ≈20 times higher than that the resistivity of bulk Cu. Indeed, such R_{on} value is observed experimentally at $I_{cc} = 10$ µA. Given that the mass density of Cu is 9.0 g cm^{-3} and that of Ta_2O_5 8.2 g cm^{-3}, then the mass density of the filament has to lie somewhere in-between, say at 8.5 g cm^{-3}, the total mass of Cu NF comes to 4×10^{-17}g. The specific heat capacity of Cu NF must also lie between the heat capacity of Cu of 0.385 J (g^{-1} °K^{-1}) and that of Ta_2O_5 of ≈750 J (g^{-1} °K^{-1}). Assuming the extreme case of 750 J (g^{-1} °K^{-1}) and using Equation (5), one can calculate the temperature difference ΔT needed to store such energy within the nanofilament alone. The temperature difference relative to the room temperature comes to at least 3×10^8 °K, which is ten times higher than the sun's core temperature of 2.7×10^7 °K. Assuming the other extreme of the specific heat capacity being c_s(Cu-CF) = 0.385 J (g^{-1} °K^{-1}), the temperature would be at 3×10^{11} °K even higher. Because this is impossible, it is clear that this kind of energy cannot be stored in the filament because of its exceedingly tiny volume. The heat instead has to be stored at least in the two (Cu and Pt) electrodes, by the dominant heat conduction transfer, and in the filament whose volume contribution can be neglected. In addition, since, the electrodes have a very large surface to volume ratio, a large part of energy delivered to the electrodes will be dissipated due to Newtonian losses, including radiation and buoyancy-driven convection.[38] Thus, one may assume that over one heating period during the reset operation, only a fraction of Q_{JH} will really be stored in the electrode material, or $Q_{st} = Q_{JH} \times f_{loss}$, where f_{loss} denotes a fraction of the heat retained in the material after all heat losses to the ambient. The coefficient f_{loss} can be related to the coefficient of heat transfer, r, to the ambient, $f_{loss} \approx \exp(-rt)$.[39] When a memory cell is switched back and forth in quick succession N times, the heat, Q_{Nst}, stored in the electrodes is given in Equation (6)

$$Q_{Nst} = N \times Q_{st} \times f_{diss} = N \times Q_{JH} \times f_{loss} \times f_{diss} = c_s \times m \times \Delta T \quad (6)$$

Where f_{diss}, is a factor smaller than unity describing the dissipation time between the switching cycles and accounting also for the cool-off period during the set operation when no current is flowing or very small current limited by I_{cc} and by the heat loss when transported between the heated and probed neighboring cells. m in Equation (6) is now the total mass of the two electrodes connected by the filament.

For an evaluation of Equation (6), we possess an important experimental reference. Under certain switching conditions for medium-to-large R_{on} and small rr, chosen deliberately in order to maximize the heating, when a cell is switched on and off repeatedly, we observe melting of the Cu electrode over the heated cell extending even to the contact pads as shown in **Figure 6**. In Figure 6a, the melting of the top Cu electrode over the ReRAM cell is shown. Because of the high thermal diffusivity, the high temperature spreads even to the contact pad as shown in Figure 6b and distorts their square shape visibly while the contact pads for the Pt electrodes remain intact. In this context, we observe that the Cu electrode line runs entirely over a thin 25 nm TaO_x but the Cu pads are located on a 730 nm SiO_2 field oxide. In addition, underneath the TaO_x layer, there is an array of Pt electrode lines which appears to indicate that the heat transfer from the Cu electrode through the thin TaO_x with the Pt lines underneath is more efficient in heat transport than through the thick SiO_2 field oxide. Hence, after several heating cycles the temperature of the pad is higher than the temperature of the electrode line.

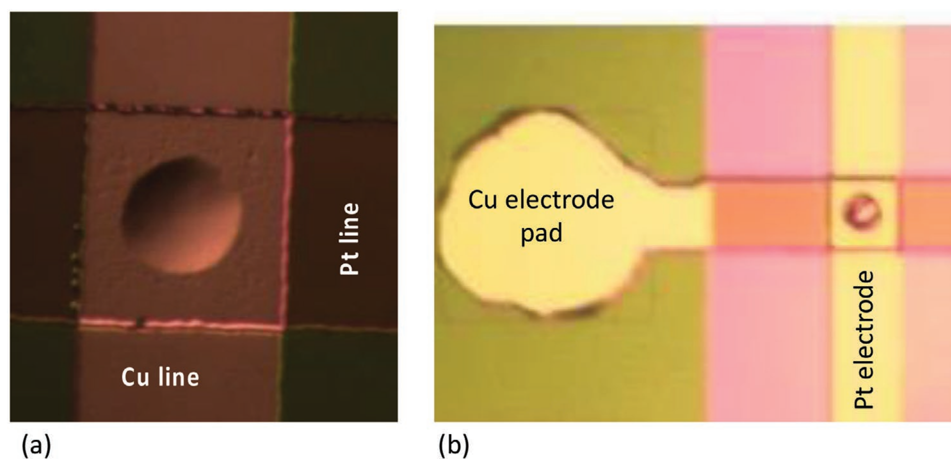

Figure 6. Optical microscope picture of the segments of the memory array showing: a) local melting of the Cu electrode over the heat-stressed ReRAM cell, and b) the heat from the ReRAM cell driven to the melting of Cu electrode is transferred to the pad showing severe distortions.

 © 2023 The Authors. Advanced Electronic Materials published by Wiley-VCH GmbH

2199160x, 0, Downloaded from https://onlinelibrary.wiley.com/doi/10.1002/aelm.202201081 by Virginia Tech, Wiley Online Library on [23/03/2023]. See the Terms and Conditions (https://onlinelibrary.wiley.com/terms-and-conditions) on Wiley Online Library for rules of use; OA articles are governed by the applicable Creative Commons License

This particular melting of Cu electrode has been observed for 25 switching cycles, each cycle being characterized by Q_{JH} = 40 µJ, according to the values used for rr, and experimental values for R_{on} and for V_{reset}. Since the melting of Cu occurs at 1085 °C for Cu layers thicker than 100 nm,[40] we can calculate from Equation (6) the product $f_{loss} \times f_{diss}$ using the specific heat capacities for Cu, c_s = 0.385 K (g^{-1} °K^{-1}), and for Pt c_s = 0.13 J (g^{-1} °K^{-1}), and obtain $f_{loss} \times f_{diss} = 0.063$.

With this information, one can now go back and calculate what is the average temperature increase in the CF-electrodes system after one single switching cycle used for the experiments shown in Table 3 for which one reset cycle has Q_{JH} = 10 µJ. Thus, we can repeat the calculation using Equation (6), but now taking as a mass, the entire mass of the Cu and Pt electrodes including the contact pads of square shape with 100 µm on the side, and using the respective specific heat capacities for Cu: c_s = 0.385 K J^{-1} (g^{-1} °K^{-1}) and for Pt: c_s = 0.13 J (g^{-1} °K^{-1}) and calculate the ΔT. Using Q_{JH} = 10 µJ, f_{loss} = 0.1, we obtain from the dimensions of our ReRAM array ΔT = 27 °C, assuming that the heat is uniformly distributed. Naturally, the temperature, at least initially, when the heated cell is only being heated, is not uniform, but as stated before, because of the high thermal diffusivity, reaches such state within a short time period. As the heat spreads from the heated cell to other cells the maximum temperature of the neighboring cell will be lower.

One can reliably estimate f_{diss} from the solution of 1-D heat equation for an isolated metal rod:[41]

$$\frac{\partial T}{\partial t} = k\frac{\partial^2 T}{\partial x^2} + \frac{p}{c_s \rho} \tag{7}$$

Where T is the temperature, k is the thermal diffusivity, p is the heat provided, c_s is the specific heat capacity, and ρ is the mass density. Equation (7) for the metallic rod with one end being heated has been solved explicitly.[41] It is noted that the thermal diffusivities of Cu and Pt are substantially higher than for TaO_x of k = 0.02 cm^2 s^{-1}, (see Table 1).

The characteristic time scale for the Equation (7) is given by $t_{ts} = L^2/k$. If one takes as a typical distance L the space between two electrodes, i.e., 150 µm and the thermal diffusivity k of Cu of 1.11cm^2 s^{-1}, one obtains t_{ts} = 200 µs. Since the pulse period of our set-reset cycles is 60 s, which is 3×10^5 times larger than t_{ts}, one may evaluate Equation (7) under steady state condition. In the steady state condition the temperature is a linear function of the space coordinate. Of course, during the period of 60 s, the electrode is cooling off due to the Newtonian losses and the fraction of the heat remaining in the electrode is estimated by the factor f_{loss} as described before. Thus, assuming that the electrode is heated by a cell at one end, the temperature along the electrode varies linearly.

From the equation $L = \sqrt{k \times t_{tr}}$, one can estimate the time, t_{tr}, required for a temperature front to move over the length L = 850 µm, from the heated cell to the far-off pad of the electrode. For the Cu electrode, this time is smaller than 10 ms, and larger for the Pt electrode, due to its five times smaller thermal diffusivity (Table 1). From this, it is clear that for the neighboring cells being characterized after the heating of the heated cell has been stopped for 40–60 s, the temperature distribution may well be represented by a steady state, which according to the solution of Equation (7) for a perfectly insulated metal rod is linear function of temperature as a function the longitudinal spatial coordinate, x, of the electrode.

Since in steady state the temperature is a linear function of location, assuming that the first cell on the electrode has been heated and has reached temperature T_c while the far end pad of the electrode is at $T_o < T_c$, then the temperature drop from cell to cell is given by (T_c-T_o) × 150/(5 × 150+100) = (T_c-T_o) × 0.18, where 150 denotes 150 µm distance between two cells and 5 × 150 + 100 = 850 µm is the distance of the heated cell from the far end contact pad. In the initial stage of heating one can assume that T_o is still at 27 °C.

Counting the heat loss traveling to further neighboring cells a good estimate for f_{diss} is 0.6-0.7. Using the experimental finding $f_{loss} \times f_{diss} = 0.063$ the latter result allows one to estimate f_{loss} as 0.11-0.09 which justifies our use of f_{loss} = 0.1 above. Thus the critical temperature of the heated cell drops to lower values as the heat is being transferred along the common electrode to the neighboring cells.

The critical temperature itself, T_c, at which one cell becomes unstable, depends on the robustness of the Cu CF and, hence, it increases with the strength of the filament. For a fragile filament with R_{on} of several tens of kΩ, the critical cell temperature will be as low 350 °C. The temperature of 350 °C can be estimated from number of cycles leading to a rupture of a given Cu filament. From our heating experiments of a probed cell with a strong Cu filament of R_{on} = 5kΩ set at I_{cc} = 100 µA, 25 cycles of heating of the heated cell were needed to observe the onset of the melting of the Cu electrode pads. This allows one to estimate ΔT for a single cycle ΔT = (1085 °C–27 °C)/25 = 42 °C. Subsequently, we have repeated the experiment with the same heated cell but the probed cell was set at much weaker filament of R_{on} = 20kΩ set at I_{cc} = 20 µA, and 7–8 cycles of heating were sufficient to rupture the cell. Since one cycle raises the temperature by 42 °C, then 42 °C × 8 + 25 °C = 361 °C. Thus a critical temperature to rupture the weaker Cu filament is ≈350 °C.

But a strong Cu filament, with low resistance of several hundred Ohm, will exhibit a critical temperature close to melting temperature of Cu, i.e., 1085 °C, as demonstrated in the experiment shown in Figure 6. In **Figure 7**, we plot the critical temperature for a weak filament for all 5 cells disposed along the Pt line, with the first cell being the heated cell and the remaining the neighbor cells being remotely heated. The heated cell is heated with 13 maximum heating switching cycles to reach T_c = 350 °C and the neighboring cells will exhibit lower temperatures, $T_c \times f_{diss}$, $T_c \times f_{diss}^2$, $T_c \times f_{diss}^3$, $T_c \times f_{diss}^4$, for the 1st, 2nd, 3rd, and 4th neighbor, respectively as discussed above.

In Figure 7, for every neighbor cell, the temperature difference of the cell to T_c is also indicated. According to Sato et al.,[32] the temperature in the reset process reaches the same temperature in each reset, thus it is bound to reach the same T_c, at which further switching is not possible. If one divides the critical temperature T_c by the temperature difference of ΔT = 27 °C, the temperature increase due to one switching cycle, one can calculate M_x of cycles that a remotely heated neighboring cell may switch. These numbers are also indicated in Figure 7; for example for the 1st neighboring cell one obtains 130/27 = 4.81, indicating that the cell can be switched for 4–5 more cycles, at most. If one compares the predicted number of additional

© 2023 The Authors. Advanced Electronic Materials published by Wiley-VCH GmbH

2199160x, 0, Downloaded from https://onlinelibrary.wiley.com/doi/10.1002/aelm.202201081 by Virginia Tech, Wiley Online Library on [23/03/2023]. See the Terms and Conditions (https://onlinelibrary.wiley.com/terms-and-conditions) on Wiley Online Library for rules of use; OA articles are governed by the applicable Creative Commons License

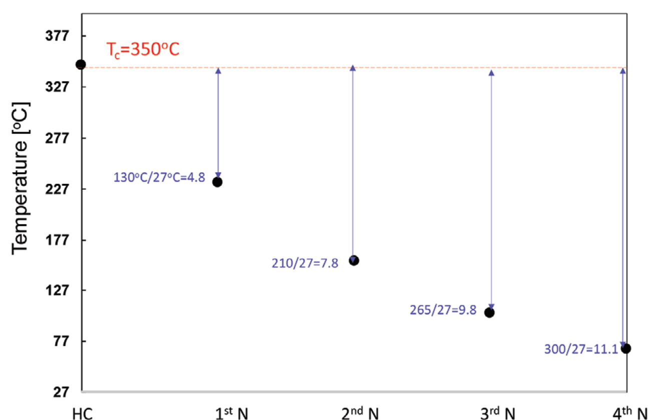

Figure 7. Shows the temperature of the four neighboring cells heated by the heated cell HC. The HC cell reaches critical temperature T_c for the cell and heats remotely the neighboring cells. The difference between T_c and actual temperature of the neighboring cell indicates how many times the cell can be switched to reach T_c. This difference divided by the ΔT (here 27 °C) of each heating cycle, indicates the maximum number of switching cycles.

switching cycles with the corresponding experimental numbers M_x(ave) in Table 3, one finds a remarkable agreement.

One can test the predictive power of the above methodology by manufacturing ReRAM arrays with enhanced thermal properties of the electrodes. We have accomplished this by replacing the inert electrode of Pt(50 nm) by Rh(50 nm), and by the composite electrodes Pt(50 nm)/Cu(100 nm) and Pt(50 nm)/Cu(200 nm). The relevant material properties of the materials used are summarized in Table 1. Two important properties of the bottom inert electrode are being changed, the thermal conductivity is enhanced by a factor of 4, the product $m \times c_s$ increases in case of the added 200 nm Cu layer by a factor of 1.95, and in case of the added 100 nm Cu layer by a factor of 1.47. Repeating now the same electric characterization experiments of the degraded cells using the same parameters for Q_{JH}, we can calculate the ΔT for a single heating cycle. For the Pt(50 nm) array, we obtained ΔT = 26.5 °C and for Pt(50 nm)/Cu(100 nm), we can predict a ΔT = 18.0 °C, and for Pt(50 nm)/Cu(200 nm) a ΔT = 13.5 °C. Clearly with the enhanced capacity of the bottom electrode to store heat, the number of heating cycles to reach the same T_c, or to render the cell inoperable, is bound to increase. The maximum number of switching cycles will increase even more, on account of the much higher thermal conductivity of the bottom electrode which allows a much faster spread of the heat pulse along the electrode.

The thermal conductivity of the composite inert electrode Pt(50 nm)/Cu(200 nm) increased more than fivefold leading to a fivefold increase of thermal diffusivity, the f_{diss} should be smaller than for the Pt(50 nm) by a factor at least 3–4 times. This would indicate that for the new array for the same switching parameters, the maximum number of switching steps should be 6 to 8 times larger, 78–104 maximum switching cycles. For the case of an array with Pt(50 nm)/Cu(100 nm), the corresponding quantities are ΔT = 18.0 °C and the maximum switching cycles of ≈26. The data of maximum switching cycles for the two Pt/Cu inert electrodes and for the Rh electrode is shown in **Table 4**. The analogous electric characterization

Table 4. Maximum number, Mx, of switching cycles for a fragile Cu nanofilament, in ReRAM arrays with different inert electrodes: Pt(50 nm), Rh(50 nm), Pt(50 nm)/Cu(100 nm), and Pt(50 nm)/Cu(200 nm) as shown in Figure 3.

ReRAM	Pt [50 nm]	Rh [50 nm]	Pt [50 nm]/Cu [100 nm]	Pt [50 nm]/Cu [200 nm]
M_x	13	26	25	75

experiments performed on Pt(50 nm)/Cu(100 nm) and Pt(50 nm)/Cu(200 nm) arrays in the same as the experiments on the Pt(50 nm) array show that the maximum number of cycles to reach the state of cell's inoperability increases as shown in **Table 5** and **Table 6**, confirming very accurately the predictions based on the previous thermal analysis, as shown in Table 5 and Table 6 for the Pt(50 nm)/Cu(100 nm) and Pt(50 nm)/Cu(200 nm), respectively.

From Table 5 and 6, it is clearly seen that with higher specific heat capacity and higher thermal conductivity of the bottom inert electrode, the electric performance degradation decreased drastically. In case of the Pt(50 nm)/Cu(200 nm) inert electrode, no degradation at all of the cells disposed along the Pt electrode is observed, and, in case of the devices along the Cu electrode, only the first neighbor suffers a low degradation of 11%. Clearly the higher thermal conductivity and specific heat capacity lead to much smaller local temperature than for the Pt(50 nm)/Ti(30 nm) ReRAM array. In case of Pt(50 nm)/Cu(200 nm), this kind of experimental characterization performed for this work is rather tedious because the cells that fail for a Pt(50 nm) electrode only after 13 times, but for Pt(50 nm)/Cu(200 nm) switch now for 72–90 times, requiring a lot of student's time.

The proposed thermal analysis can also be extended to the dependence of cell degradation on the width of the line of the same ReRAM array. With the increase of the width, the volume of the electrode increases proportionally and thus, according to Equation (5) the temperature difference ΔT decreases. Our experiments so far have been using 10 µm Cu and Pt lines as a standard. We have repeated the analysis for the Pt(50 nm) ReRAM array for a 35 µm wide Pt line. Clearly, the mass of the Pt electrode increased by a factor of 3.5 and the total product $m \times c_s$ increased by a factor of 1.59 about the same as the product $m \times c_s$ for the Pt(50 nm) 10 µm electrode. However, the thermal conductivity remained the same, because the Pt material did not change. The electrical characterization of the 35 µm wide Pt line of the Pt(50 nm) array, shown in **Table 7**, shows that the degradation of the neighboring cells is smaller than for the 10 µm Pt line of the Pt(50 nm) arrays but somewhat worse than for the Pt(50 nm)/Cu(100 nm) ReRAM array.

Table 7 confirms further the validity of the thermal analysis and the accuracy of its predictions. In addition, in an earlier

Table 5. Degradation D of the neighbor cells of the heated device for the array with inert electrode of Pt(50 nm)/Cu(100 nm) array for a 10 µm wide line.

	Neighbor cell to the heated cell along Pt(50 nm)/Cu(100 nm) metal line				Neighbor cell to the heated cell along Cu metal line			
#neighbor	1st	2nd	3rd	4th	1st	2nd	3rd	4th
D [%]	23	1	0	0	57	41	0	0

 © 2023 The Authors. Advanced Electronic Materials published by Wiley-VCH GmbH

2199160x, 0, Downloaded from https://onlinelibrary.wiley.com/doi/10.1002/aelm.202201081 by Virginia Tech, Wiley Online Library on [23/03/2023]. See the Terms and Conditions (https://onlinelibrary.wiley.com/terms-and-conditions) on Wiley Online Library for rules of use; OA articles are governed by the applicable Creative Commons License

ADVANCED ELECTRONIC MATERIALS
Open Access
www.advelectronicmat.de

2199160x, 0, Downloaded from https://onlinelibrary.wiley.com/doi/10.1002/aelm.202201081 by Virginia Tech, Wiley Online Library on [23/03/2023]. See the Terms and Conditions (https://onlinelibrary.wiley.com/terms-and-conditions) on Wiley Online Library for rules of use; OA articles are governed by the applicable Creative Commons License

Table 6. Degradation D of the neighbor cells of the heated device for the array with inert electrode of Pt(50 nm)/Cu(200 nm) array for a 10 µm wide line.

	Neighbor cell to the heated cell along Pt(50 nm)/Cu(200 nm) metal line				Neighbor cell to the heated cell along Cu metal line			
#neighbor	1st	2nd	3rd	4th	1st	2nd	3rd	4th
D [%]	0	0	0	0	11	0	0	0

work,[18] we have found that for the same switching conditions a ReRAM where the Pt(50 nm)/Ti(30 nm) electrode has been replaced by Rh(50 nm)/Cr(30 nm) electrode displays almost exactly the same electric characteristics as for Cu/TaO_x/Pt/Ti. However, a cell set at I_{cc} = 10 µA with M_x of 15 for Pt/Ti increases to 26 for Rh/Cr devices. This can be attributed to the higher thermal conductivity of Rh (150 W mK^{-1}) and Cr (94 W mK^{-1}) versus Pt (72 W mK^{-1}) and Ti (22 W mK^{-1}) with Ti and Cr layers of 20 nm serving as glue layers. In our thermal analysis, we find that the $m \times c_s$ for Rh and Pt electrode are similar, with the product for Rh being only slightly higher than that of Pt (see Table 2). But the thermal conductivity of Rh is a factor 2 larger than for Pt, so we expect the temperature of the neighboring cells lower in case of Rh electrode than for the Pt electrode. The experimentally found enhancement factor of 26/15 = 1.73 lies in the reasonable range of the estimates of the thermal analysis proposed here. The case of the Rh(50 nm) electrode is, in a sense, an opposite to the case of a wider Pt (35 µm) electrode. In case of a wider Pt line the product $m \times c_s$ increased by a factor of 3.5, but the thermal conductivity was the same compared with Pt line of 10 µm width. In case of Rh 10 µm electrode, the product $m \times c_s$ is the same, but the thermal conductivity increased by a factor of 2.

Furthermore, in Figure 2, two identical devices Cu/TaO_x/Ru have been fitted with different glue layers Ti and Cr. The main reason why Ti has been replaced with Cr is Cr's almost fivefold higher thermal conductivity 94 W mK^{-1} than for Ti of 18 W mK^{-1}. One finds that the electric performance of nominally identical devices depends sensitively on the nature of the glue layer. We find that the V_{reset} value for Ru/Cr is 0.4 V larger ($V_{reset(Ru/Cr)}$ = –3.8 V) than for the Ru/Ti device ($V_{reset(Ru/Ti)}$ = –3.4 V). Such result was, in fact, expected based on our analysis. The device Ru/Cr experiences much higher heat removal rate from the Cu CF during the reset operation than the Ru/Ti device. In case of Ru/Ti, the Joules heat generated in the filament cannot be as easily dissipated and lingers therefore for some time around the hot spot in the filament. Thus, lower thermal conductivity of the inert electrode requires less Joules heating than an inert electrode with high thermal conductivity as the heat accumulates in the nanofilament in a shorter time than in the case of high thermal conductivity of the inert electrode, and hence lower V_{reset} voltage. It is also instructive to compare V_{reset} values of the other devices. We find V_{reset} for Co/Ti and Pt/Ti device, to be V_{reset}(Pt/Ti) = –0.9 V, V_{reset}(Co/Ti) = –1.0 V or essentially the same, which correlates again very well with the same thermal conductivities of the two metals of 69 W Km^{-1}. Finally there is large difference between the V_{reset} for Ru devices and Pt and Co devices of ≈2.5 V, which is in perfect agreement with the much higher thermal conductivity of Ru compared with Pt and Co devices.

It has been thus amply demonstrated that three mechanisms: (i) the thermal conductivity, (ii) the material's capacity per degree K to absorb heat or $m \times c_s$, and (iii) the geometry of the electrodes, contribute in almost equal ways to the effects of the thermal cross-talk on the device performance. Once calibrated to a base line array, our methodology can quantitatively predict the improvement or worsening of the degradation effect in terms of material properties and geometry parameters.

Finally, we wish to comment on the cycling ability of various devices. Although initially Cu/TaO_x/Pt and Cu/TaO_x/Ru devices behave similarly, albeit with different V_{form}, V_{set}, and V_{reset} threshold voltages, the main difference between the two devices is the cycling ability which in case of Ru devices is very limited.[25] At most stable switching conditions the Pt device could undergo upward of hundred switching cycles, while the Ru device's cycling ability was limited to 13 cycles. The limited cycling ability was found to be caused by the degraded inertness properties of the Ru electrode. Similarly, it has been shown that Cu/TaO_x/Ti and Cu/TaO_x/Ta devices displayed very limited switching capability compared with Cu/TaO_x/Pt devices.[42] The limited cycling ability was attributed to reduced stopping power of the counter-electrode (dissolution of cations in the counter-electrode), to reduced cation nucleation rate at the counter-electrode, and to reactivity of Ti and Ta inert electrode metals with the dielectric of the switching layer.

5. Conclusions

In conclusion, we have presented ample experimental evidence of how material properties and geometries of the ReRAM electrodes impact the intensity of thermal cross-talk and how the thermal cross-talk, in turn, impacts the various manifestations of electrical performance degradation of the resistive memory cells. A comprehensive thermal analysis of the thermal cross-talk has been provided which quantifies the amount of device degradation in terms materials properties such as thermal conductivity, specific heat capacity, thermal diffusivity, and mass density of the electrode materials. Since the degradation effects can be described in terms of basic material properties, our

Table 7. Degradation D of the neighbor cells of the heated device for the array with inert electrode of Pt(50 nm) array for a 35 µm wide line.

	Neighbor cell to the heated cell along Pt(50 nm) 35 µm metal line				Neighbor cell to the heated cell along 35 µm Cu metal line			
#neighbor	1st	2nd	3rd	4th	1st	2nd	3rd	4th
D [%]	43	31	19	70	65	52	40	33

© 2023 The Authors. Advanced Electronic Materials published by Wiley-VCH GmbH

ADVANCED ELECTRONIC MATERIALS
Open Access
www.advelectronicmat.de

academic memory arrays which conform with commercial arrays only in the dimensions of the layer thickness, but are much larger in lateral dimensions, still provide an excellent baseline to extract reliably the underlying physics valid also for the high density commercial ReRAM arrays. The Joule heat density in commercial cutting edge memory arrays is much more severe, about two orders of magnitude higher than in our memory arrays.[19] Hence, the presented thermal analysis may serve as reliable guide in material selection in an effort to mitigate ReRAM degradation and reliability issues caused by thermal-cross-talk. The question as to what may be the optimum choices for the inert electrode is still not satisfactorily resolved. In terms of thermal cross-talk, low electrical conductivity material leads to lower V_{reset} values – which is clearly an advantage – and distant neighboring cells are little affected by the slow heat transfer along the line. On the other hand, the heat lingers longer in the cell and in the electrode with low thermal conductivity. In case of an electrode with high thermal conductivity, the heat is dissipated faster, but now even distant neighboring cells are affected by the heat transfer. The optimum design of ReRAM memory array must take into consideration how the memory is being operated.

Acknowledgements

The research leading to this work was supported by a Semiconductor Research Corporation grant # 444234.

Conflict of Interest

The authors declare no conflict of interest.

Data Availability Statement

The data that support the findings of this study are available from the corresponding author upon reasonable request.

Keywords

reliability, resistive RAM, specific heat capacity, thermal conductivity, thermal cross-talk

Received: November 10, 2022
Revised: December 18, 2022
Published online:

[1] H. An, M. S. Al-Mamun, M. K. Orlowski, L. Liu, Y. Yi, *IEEE Trans. Comput.-Aided Des. Integr. Circuits Syst.* **2020**, *40*, 574.
[2] T. Liu, Y. Kang, S. El-Helw, T. Potnis, M. Orlowski, *Jpn. J. Appl. Phys.* **2013**, *52*, 084202.
[3] S. De, T. M. Higgins, P. E. Lyons, E. M. Doherty, P. N. Nirmalraj, W. J. Blau, J. J. Boland, J. N. Coleman, *ACS Nano* **2009**, *3*, 1767.
[4] L. Hu, H. S. Kim, J.-Y. Lee, P. Peumans, Y. Cui, *ACS Nano* **2010**, *4*, 2955.
[5] L. Yang, T. Zhang, H. Zhou, S. C. Price, B. J. Wiley, W. You, *ACS Appl. Mater. Interfaces* **2011**, *3*, 4075.
[6] G. Zhou, Z. Wang, B. Sun, F. Zhou, L. Sun, H. Zhao, X. Hu, X. Peng, J. Yan, H. Wang, W. Wang, J. Li, B. Yan, D. Kuang, Y. Wang, L. Wang, S. Duan, *Adv. Electronic Mater.* **2022**, *8*, 2101127.
[7] G. Zhou, X. Ji, F. Zhou, Z. Dong, B. Yan, B. Sun, W. Wang, X. Hu, Q. Song, L. Wang, S. Duan, *iScience* **2022**, *25*, 105240.
[8] Z. Yu, Q. Zhang, L. Li, Q. Chen, X. Niu, J. Liu, Q. Pei, *Adv. Mater.* **2011**, *23*, 664.
[9] X.-Y. Zeng, Q.-K. Zhang, R.-M. Yu, C.-Z. Lu, *Adv. Mater.* **2010**, *22*, 4484.
[10] P. Sun, N. Lu, L. Li, Y. Li, H. Wang, H. Lv, Q. Liu, S. Long, S. Liu, M. Liu, *Sci. Rep.* **2015**, *5*, 13504.
[11] R. Waser, R. Dittmann, G. Staikov, K. Szot, *Adv. Mater.* **2009**, *21*, 2632.
[12] U. Russo, D. Ielmini, C. Cagli, A. L. Lacaita, *IEEE Trans. Electron Devices* **2009**, *56*, 193.
[13] N. Mosso, A. Prasmusinto, A. Gemma, U. Drechsler, L. Novotny, B. Gotsmann, *Appl. Phys. Lett.* **2019**, *114*, 123102.
[14] S. H. Chang, S. C. Chae, S. B. Lee, C. Liu, T. W. Noh, J. S. Lee, B. Kahng, J. H. Jang, M. Y. Kim, D.-W. Kim, C. U. Jung, *Appl. Phys. Lett.* **2008**, *92*, 183507.
[15] C. Walczyk, D. Walczyk, T. Schroeder, T. Bertraud, M. Sowinska, M. Lukosius, M. Fraschke, D. Wolansky, B. Tillack, E. Miranda, C. Wenger, *IEEE Trans. Electron Devices* **2011**, *58*, 3124.
[16] M. Terai, M. Saitoh, T. Nagumo, Y. Sakotsubo, Y. Yabe, K. Takeda, T. Hase, in *Symposia on VLSI Technology*, IEEE, XX **2011**.
[17] J. S. Lee, S. Lee, T. W. Noh, *Appl. Phys. Rev.* **2015**, *2*, 031303.
[18] M. Al-Mamun, M. Orlowski, *MRS Adv.* **2019**, *4*, 2593.
[19] M. Al-Mamun, M. Orlowski, *J. Appl. Phys.* **2021**, *129*, 055107.
[20] M. Al-Mamun, M. Orlowski, *Sci. Rep.* **2021**, *11*, 7413.
[21] Y. Kang, T. Liu, T. Potnis, M. K. Orlowski, *ECS Solid State Lett.* **2013**, *2*, Q54.
[22] G. Zhou, S. Duan, P. Li, B. Sun, B. Wu, Y. Yao, X. Yang, J. Han, J. Wu, G. Wang, L. Liao, C. Lin, W. Hu, C. Xu, D. Liu, T. Chen, L. Chen, A. Zhou, Q. Song, *Adv. Electron. Mater.* **2018**, *4*, 1700567.
[23] T. Liu, M. Verma, Y. Kang, M. Orlowski, *Appl. Phys. Lett.* **2012**, *101*, 073510.
[24] A. Sawa, *Mater. Today* **2008**, *11*, 28.
[25] M. Al-Mamun, S. W. King, M. Orlowski, *ECS J. Solid State Sci. Technol.* **2019**, *8*, N220.
[26] P. R. Mickel, A. J. Lohn, M. J. Marinella, *Appl. Phys. Lett.* **2014**, *105*, 053503.
[27] P. R. Mickel, A. J. Lohn, C. D. James, M. J. Marinella, *Adv. Mat.* **2014**, *26*, 4486.
[28] P. Sun, L. Li, N. Lu, Y. Li, M. Wang, H. Xie, S. Liu, M. Liu, *J. Comput. Electron.* **2014**, *13*, 432.
[29] D. Niraula, V. G. Karpov, *IEEE Trans. Electron Devices* **2017**, *64*, 4106.
[30] H. Fangohr, D. S. Chernyshenko, M. Franchin, T. Fischbacher, G. Meier, *Phys. Rev. B* **2011**, *84*, 054437.
[31] M. Uenuma, Y. Ishikawa, Y. Uraoka, *Appl. Phys. Lett.* **2015**, *107*, 073503.
[32] Y. Sato, K. Kinoshita, M. Aoki, Y. Sugiyama, *Appl. Phys. Lett.* **2007**, *90*, 033503.
[33] E. Linn, R. Rosezin, C. Kügeler, R. Waser, *Nat. Mater.* **2010**, *9*, 403.
[34] G. Ghosh, M. Orlowski, *IEEE Trans. Electron Devices* **2015**, *62*, 2850.
[35] G. Ghosh, M. K. Orlowski, *Curr. Appl. Phys.* **2015**, *15*, 1124.
[36] G. K. White, S. J. Collocott, *J. Phys. Chem. Ref. Data* **1984**, *13*, 1251.
[37] Y. Fan, M. A.- Mamun, B. Conlon, S. W. King, M. K. Orlowski, *ECS Trans.* **2017**, *75*, 13.
[38] I. Rafols, J. Ortin, *Am. J. Phys.* **1992**, *60*, 846.
[39] J. H. Lienhard, *A Heat Transfer Textbook*, 5th ed., Dover Publications, Mineola, New York **2019**.
[40] M.-L. Liao, I.-L. Chang, F.-R. Chang, *J. Mater. Res.* **2014**, *29*, 535.
[41] E. M. Stein, R. Shakarchi, *Fourier Analysis*, Princeton University Press, XX **2003**, pp. 750-770.
[42] G. Ghosh, Y. Kang, S. W. King, M. Orlowski, *ECS J. Solid State Sci. Technol.* **2017**, *6*, N1.

© 2023 The Authors. Advanced Electronic Materials published by Wiley-VCH GmbH

2199160x, 0, Downloaded from https://onlinelibrary.wiley.com/doi/10.1002/aelm.202201081 by Virginia Tech, Wiley Online Library on [23/03/2023]. See the Terms and Conditions (https://onlinelibrary.wiley.com/terms-and-conditions) on Wiley Online Library for rules of use; OA articles are governed by the applicable Creative Commons License